# Prediction And Exploitation: The use of the *EOSTAR* model in the marine infrared propagation environment

S. M. Doss-Hammel, D. Tsintikidis
SPAWAR Systems Center, San Diego CA
stephen.doss-hammel@navy.mil

A. M. J. van Eijk, G. J. Kunz
TNO Physics and Electronics Laboratory, The Hague, The Netherlands

October 9, 2003

**Abstract**

Modern surface Navy ships require dependable and predictable communications, surveillance, and tracking systems. An accurate model for the propagation of infrared and optical frequencies through the atmosphere is a requirement for these systems, which operate over long nearly-horizontal paths that are close to the land or sea surface.

The determination of the propagation environment for surface ships can be a difficult problem. The most critical portion is the 50-meter-thick surface layer containing the ship and extending to the horizon. Extended horizontal propagation paths within this atmospheric surface layer encounter relatively dynamic refractivity conditions.

We will describe the application of the *EOSTAR* (Electro-Optical Signal Transmission and Ranging) model suite to provide accurate sensor performance predictions. The *EOSTAR* model is built upon a geometrical optics approach to infrared propagation: a ray is traced through the propagation environment, and path-dependent perturbations to the signal can be determined. *EOSTAR* is a valuable tool for prediction and exploitation of several phenomena common to this environment, and we will discuss the design and use of three individual modules within the *EOSTAR* suite: 1. Exploitation of a sub-refractive mirage to provide a passive ranging capability; 2. A path-dependent calculation of a refractive propagation factor, or geometric gain; 3. Exploitation of scintillation effects to provide an early detection capability, and the prediction of a signature frequency and variance to enable detection enhancement.

## 1 Introduction

*EOSTAR* (Electro-Optical Signal Transmission and Ranging) is a performance assessment tool for electro-optical systems. *EOSTAR* consists of a model suite to provide accurate sensor performance predictions. The *EOSTAR* model is built upon a geometrical optics

approach to infrared propagation: a ray is traced through the propagation environment, and path-dependent perturbations to the signal can be determined.

The primary computational tool for analysis of refractive effects in the *EOSTAR* model is a geometrical optics module that produces a ray-trace calculation for a given refractive environment. The ray-trace data is utilized to generate detailed information about geometrical transformations induced by the propagation environment.

### 1.1 The Vertical Temperature Profile

The geometrical optics ray-trace method is initiated by a definition of the local refractivity field. We assume that within the marine atmospheric surface layer this field can be considered to be horizontally homogeneous. For optical and infrared frequencies, the primary determinant of the refractivity profile is the vertical temperature profile.

The generation of a continuous vertical temperature profile is based upon a surface layer similarity theory developed by Monin and Obukhov. There are six different bulk models available in the *EOSTAR* suite because of the choice of three different micrometeorological models combined with two different choices for stability function.

The profile is defined in terms of the potential temperature $\theta$ which is derived from the air temperature $T$ by $\theta = T + \Gamma_d z$ where $\Gamma_d$ is the dry adiabatic lapse rate, and $z$ is height above the surface. Air temperature measurements are taken at the sea surface, and at a reference height. These sparse data are then used in a bulk model to generate a continuous vertical profile, and with a sea surface temperature given by $T_0$, the temperature $T(z)$ at a height $z$ above the water surface is given by:

$$\theta = \theta_0 + \frac{\theta_*}{k}\left[\ln(z/Z_{0\theta}) - \Psi_\theta(z/L)\right] \tag{1}$$

where $Z_{0\theta}$ is the roughness length for the temperature profile, $\theta_*$ is the potential temperature scaling parameter, and $\theta_0$ is the surface potential temperature. $L$ is the Monin-Obukhov length, and $\Psi_\theta(z/L)$ is a stability correction function.

### 1.2 The Refractivity Gradient and Ray Curvature

The optical path calculation for a ray propagating in the atmosphere requires a determination of the refractivity field. The near sea surface atmosphere is assumed to be horizontally homogeneous. The vertical structure is divided into layers, and for each layer a refractivity gradient can be determined. Our approach follows the work of Lehn [1].

A ray propagating through a medium with a gradient in refractive index will define a curved path. The refractive index $n$ is defined for visible and infrared frequencies by:

$$n = 1 + \alpha(\lambda)\frac{P}{T},$$

where $\alpha(\lambda) = (77.6 + 0.584\lambda^{-2}) \times 10^{-6}$ and $\lambda$ is the wavelength in micrometers. The refractivity gradient is

$$\frac{dn}{dz} = -\frac{\alpha(\lambda)P}{T^2}\left(g\beta + \frac{dT}{dz}\right) \tag{2}$$

for density $\rho$ and gravitational acceleration $g$, and $\beta = 3.485 \times 10^{-3}$. The curvature $\kappa$ of a ray is defined such that positive curvature means a ray is concave towards the earth:

$$\kappa = -\frac{\sin(\zeta)}{n}\frac{dn}{dz}. \tag{3}$$

$\zeta$ is the angle between the ray and the normal to the local surface tangent plane. The radius of curvature $r$ is $r = 1/\kappa$, and this yields

$$r = \frac{nT^2}{\sin(\zeta)\alpha(\lambda)\ P\ (g\beta + dT/dz)} \tag{4}$$

where $r > 0$ defines a ray that is concave down toward the earth.

For a ray-trace calculation the atmosphere is divided into concentric shells of constant thickness and constant height. Within each shell or layer, a refractivity gradient is defined as a function of the temperature gradient. We take the temperature gradient within the layer to be constant as well, and therefore the radius of curvature for each layer is a constant. The ray-trace procedure proceeds by determining the entry height $z_0$ and entry angle $\phi_0$ of a ray into a layer, where $\phi_0$ is the angle with the horizontal. The coordinate system is established to put the entry point at range $x = 0$ and height $z = z_0$. The equation for the ray trajectory in this layer is

$$z = -\frac{x^2}{2r} + x\tan\phi_0 + z_0. \tag{5}$$

An example of the ray-trace procedure and the resultant ray family is shown in fig. 1.

The algorithm described above requires an assumption of piecewise horizontal homogeneity of the refractive field: the only gradients in refractive index occur in the vertical coordinate. The assumption of piecewise horizontal homogeneity means that the computation of the ray-trace can be confined to a vertical plane. In the remainder of this paper we will restrict further to an assumption of horizontal homogeneity. The analysis is performed in this two-dimensional plane and the coordinate system is defined with the origin at mean sea level so that the receiver location is specified by the coordinates $(0, z_r)$ and the transmitter is at $(x_t, z_t)$. The local coordinate system is further transformed to bring the curved surface of mean sea level to a horizontal plane (a "flat earth" representation). Thus the $x$-axis in the two dimensional representation is the mean sea surface, and range information along the propagation path is measured in this coordinate. The $z$-axis represents the vertical offset from $z = 0$ at mean sea level.

## 2 The Transfer Map

An important application of the geometric optics approach is the calculation of the observable effects of refractive gradients. A fundamental problem is to predict the image of a source or target at a given range. This information is accessible through the calculation of

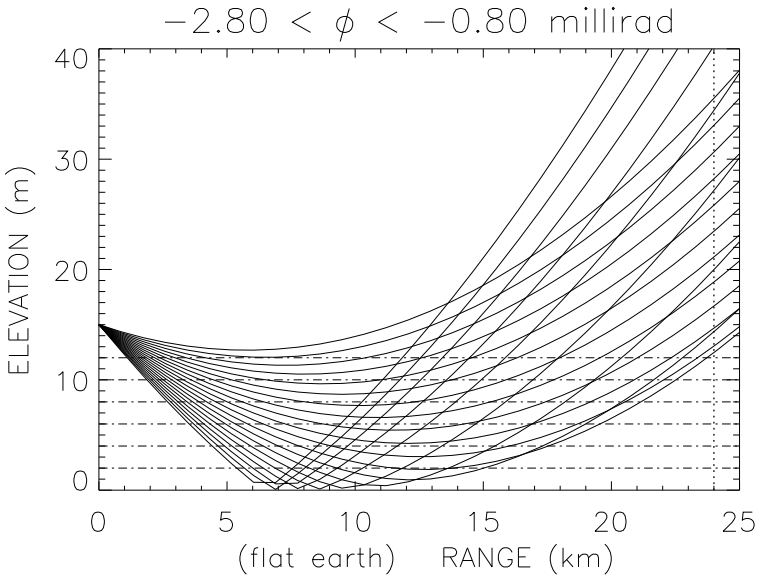


Figure 1: The vertical scale is in meters above the surface, while the horizontal scale is in kilometers downrange from the sensor which is at a height of 15 meters. The 6 horizontal dashed lines indicate constant surfaces of $2, 4, 6, 8, 10$, and $12$ meters to illustrate the passive ranging calculations (they do not define the layers of constant refractive gradient for the ray trajectory calculation). The rays that appear to be reflecting from the x-axis are actually refracted.

a transfer map within the *EOSTAR* model and we will describe this calculation along with some of its applications.

A bundle of rays is defined at a common point at the receiver to span the vertical extent of the sensor field-of-view (fig. 1). Each ray $\rho_{\text{refract}}$ is generated within the vertical plane containing the transmitter and receiver starting from the receiver location at $(0, z_r)$. Launch angles $\phi_{\text{refract}}$ are defined with respect to the ray based at $(0, x_r)$ parallel to the $x$ axis. If the source point is visible (at infrared frequency) to the receiver, we can be certain that a fan of rays defined for launch angles $-\pi/2 \leq \phi_{\text{refract}} \leq \pi/2$ will include rays that intercept the source. In practice, the computational angular extent of the fan of rays is further constrained since rays launched with a sharp downward angle will intercept the $x$-axis (earth surface) before the source range is achieved, or rays with a sharp upward launch angle will remain too high when extended to the source range. In our ray-trace procedure, there are rays $\rho_{\text{refract}}$ initiated at $(0, z_r)$ which intersect the Earth's surface (the $x$-axis) at a range $x < x_t$. These rays are terminated in the procedure: there are no reflections at Earth-surface. There exists a ray launch angle $\phi_{\min}$ with $-\pi/2 < \phi_{\min} < \pi/2$ which is the smallest angle resulting in a ray which will intersect the vertical plane.

There are three important elements that are a result of the occurrence of sub-refractive mirages:

1. the existence of a second distinct image of a source point;

2. the orientation (erect vs. inverted) of the image;

3. the local magnification in the image.

All of this information is encoded within a functional dependence of elevation angles at a selected range: $\phi_{\rm geom}(\phi_{\rm refract})$. The transfer map relationship is a map from the geometric 'atmosphere-free' angular position ($\phi_{\rm geom}$) to the refractive 'apparent' angular position ($\phi_{\rm refract}$). The transfer map is dependent upon the receiver height $z_r$ at range $x = 0$, and it is defined for a vertical plane at the range point $x = x_t$. It is determined by finding all rays $\rho_{\rm refract}$ originating at the receiver location $(0, z_r)$ which intersect a vertical plane at range $x = x_t$.

A transfer map for the ray-trace in fig. 1 is shown in fig. 2.

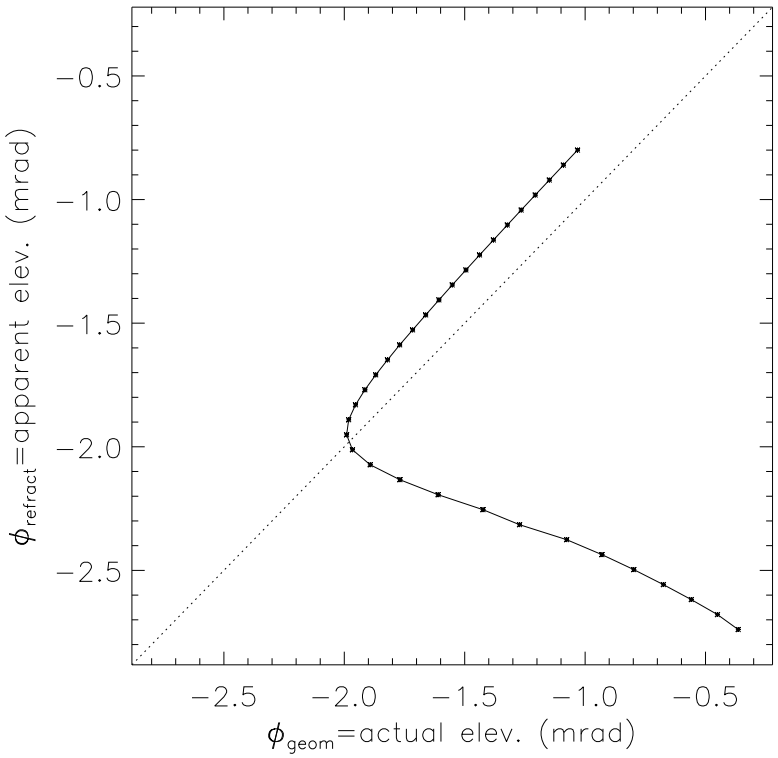


Figure 2: The transfer map is a transformation from the geometric (or atmosphere-free) actual angular position $\phi_{\rm geom}$ to the refractive apparent angular position $\phi_{\rm refract}$. This map is calculated for the ray-trace shown in fig. 1 at a range of 24 km. The dotted-line of $\phi_{\rm refract} = \phi_{\rm geom}$ indicates an identity transformation (the atmosphere-free case).

The discrete points represent a continuous curve, and the point of infinite derivative on

this curve corresponds to the caustic point in the ray-trace envelope. The three important features noted at the beginning of the section can all be determined from this map. The magnification $\delta$ of the image is determined by

$$\delta = \left| \frac{d\phi_{\text{refract}}}{d\phi_{\text{geom}}} \right| \tag{6}$$

and the orientation of the image (erect or inverted) is given by the sign of $d\phi_{\text{refract}}/d\phi_{\text{geom}}$. The point at which the graph of the transfer map (fig. 2) has infinite slope corresponds to the caustic point, and this point can also be located on the ray-trace in fig. 1 as the lowest height for all rays intersecting the vertical line at the 24 km range.

### 2.1 A visualization of the transfer map

A useful and powerful capability within the *EOSTAR* program is the display of the target plane at any range requested by the user. The ray trajectory calculation permits assessment of image distortion due to atmospheric refraction. Atmospheric refraction becomes important for long range observations. Mirage effects occur frequently over the ocean, hampering identification and affecting the maximum visibility ranges of targets and possible threats to a ship.

*EOSTAR* has a number of pre-programmed extended targets that can be placed anywhere in the user-defined space and viewed from any aspect angle to study the atmosphere effects on IR imaging. These targets are constructed from triangulated facets which can be given several properties such as temperature and spectral emission coefficient. With this information and the spectrally resolved atmospheric transmission, background radiation, and path radiation it is possible to simulate a true spectral image of a target in the scene as seen by the sensor system and to calculate the radiance or contrast for the selected aspect angle.

Thus if it is desired to see the effects of the ray-trace shown in fig. 1, the *EOSTAR* program, it is possible to open two windows that display an image at any desired range. The two windows present the image as it if transformed by the refractive effects of the atmosphere, and the image as it would appear at range without any atmospheric refractive effects. Examples of synthesized images of a representative ship in a non-refracting and in a refracting atmosphere are presented in the upper and lower panels of fig. 3 respectively. Contour lines around the elementary triangles are shown to emphasize the individual elements of the target.

Based on the calculated ray trajectories and the vertical profiles of temperature, humidity and refractive index structure parameter, *EOSTAR* calculates the path-integrated and spectrally-resolved transmission, background- and path-radiation, as well as the scintillation and blur for a point source at a selected position of a distant point target. All these data, which can be considered as third level data, are summarized in a small monitor form on the screen for easy access.

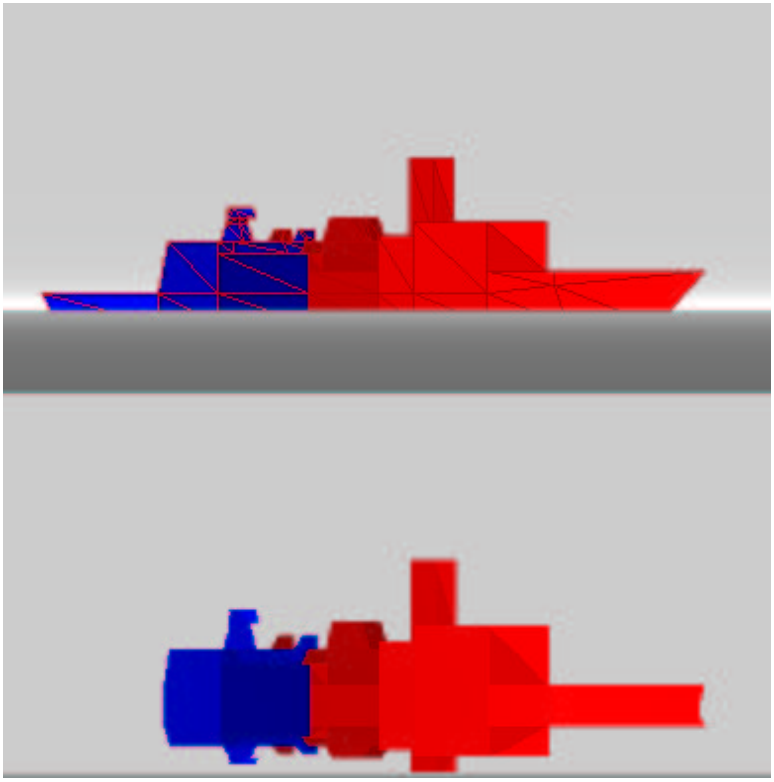

Figure 3: Two image visualizations generated by *EOSTAR*. The upper panel shows a ship target in a non-refracting atmosphere (reference view) and the lower panel shows the same target in the refracting atmosphere similar to the one defined by fig. 1. The gray band crossing horizontally indicates the ocean surface for the upper panel; in the lower panel the ocean surface elevation is reduced substantially due to refractive (mirage) effects. The images show only refractive effects, and no turbulence, transmission or radiative effects.

## 3 The Refractive Propagation Factor

An application of the transfer map calculation is the determination of a "geometric" gain, which is a change in signal intensity due entirely to the nature of the refractive field between target and sensor [2]. The propagation factor F is defined as the ratio between the actual field amplitude at a selected field point and the corresponding field amplitude at that point in free-space propagation conditions. The field intensity at the receiver is given in terms of the field amplitude propagation factor F by

$$F^2 = \sum_{\phi_{\text{refract}}} \left| \frac{d\phi_{\text{refract}}/dz}{d\phi_{\text{geom}}/dz} \right|_{(x,z)=(x_t,z_t)} \tag{7}$$

where the summation is over all values $-\pi/2 \leq \phi_{\text{refract}} \leq \pi/2$ for which rays terminate at $(x_t, y_t)$. The propagation factor is defined for piecewise horizontally homogeneous environ-

ments, and it is dependent only on the spatial locations of the source point and receiver point in space. It is therefore necessary mathematically for the definition to include the full $\pi$-radian fan of rays for $\phi_{\text{refract}}$ to ensure that all rays from a source are accounted for at the receiver. Therefore at the upper and lower summation limits, $\phi_{\text{geom}} = \phi_{\text{refract}} = \pi/2$ and $\phi_{\text{geom}} = \phi_{\text{refract}} = -\pi/2$ since it is only the vertical rays that are certain to be undeviated in a piecewise horizontally homogeneous propagation environment. In practice, the field of view of a sensor will generally be considerably less than $\pi$ radians.

A fan of rays that has been calculated for a given refractive profile can be used to deduce the refractive modifications to the observed source intensity. We use a term that is borrowed from radio-frequency propagation models, and call this multiplicative term the *refractive propagation factor*. The word "refractive" is appended to indicate that changes in field amplitude due to refractive effects are included, but *not* changes due to any reflection of the propagating beam. The refractive propagation factor is a function of both the receiver location and the transmitter location. The receiver is located by definition at zero range, so the propagation factor is a function of three parameters: receiver height $z_r$, transmitter height $z_t$, and range $x_r$.

Given the receiver height $z_r$, a two-dimensional field of values for $F^2$ is determined. At a range of $\approx 5$ km the refractive propagation factor is $F^2 \approx 1$, because the field magnification is nearly neutral (see fig. 1). After a longer propagation path, a sub-refractive mirage develops, and a second image of the transmitter becomes visible. The combined intensities from the two images result in a signal intensity greater than the freespace value. This is indicated by fig. 4 which shows a calculation of the gain-height function at a range of 24 km. The ray-trace foundation for this calculation can be seen in fig. 1 where a vertical dotted line indicates the vertical plane at a range of 24 km. In these conditions a sub-refractive mirage is visible. The plot indicates that a transmitter at a height of 11 m will not be visible, while a transmitter at 13 m will be detected with a strongly amplified signal.

The height-gain curve implies that $F^2 > 1$ for $z > 13$ m, and as height decreases from 30 m, $F^2$ increases. As height is reduced to $\approx 13$ m, $F^2$ continues to increase and becomes divergent at $z_c \approx 12.5$. This is because of the source point approach to a singularity at the caustic at a range of 24 m. This can be verified by reference to fig. 1 for which the caustic point is at the intersection of the lowest point of the ray envelope and the vertical line at range 24 km. There are methods for resolving the singularities at the caustic [3, 4] but these methods have not yet been implemented in *EOSTAR*.

# 4 Applications of the refractive propagation factor, or geometric gain

The *EOSTAR* application can provide a complete estimate of the effects of the multiple factors that modify a propagating signal. As an example, for a specified geometry and meteorological conditions, *EOSTAR* will determine the molecular extinction (using MODTRAN), the aerosol extinction (using ANAM) and the geometric gain (or refractive propagation.) Each of the processes is then compounded multiplicatively to provide an estimate

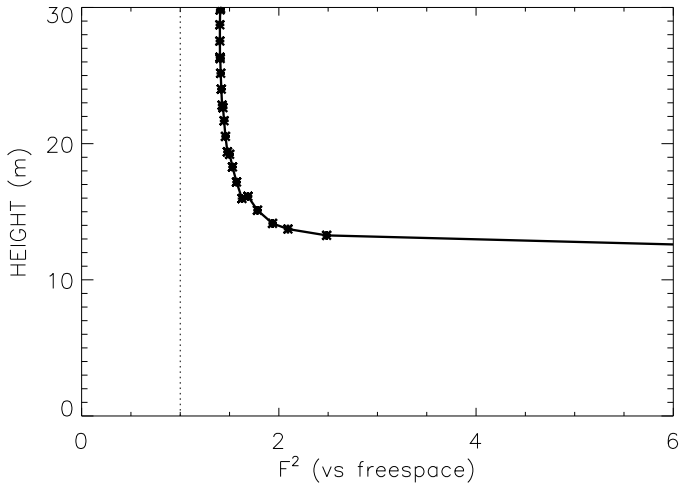


Figure 4: Gain as a function of height at a range of $\approx$ 24km. Note the large increase in gain at $\approx$ 13 m height. Below 12 m there is zero signal.

of transmission *along a specified ray*.

An illustration of the effects of mirages on the received signal strength is provided by fig. 5 The mirage prediction for the scenario portrayed in fig. 5 is somewhat idealized. A particular shortcoming is the assumption of a flat surface. This over-simplification can be rectified by inserting a surface wave field. Crests of the waves will extend above the surface boundary which defines the Monin-Obukhov theory, and interrupt the ray or beam trace. This capability exists within *EOSTAR*, and it is activated by specifying the windspeed in one of the multiple micro-meteorological models.

During the RED experiment, refractive changes in the signal intensity did not appear to be a significant factor. The test configuration geometry included a receiver near the sea surface, a source relatively high above the sea-surface, and a moderate range between the two. In addition, there were almost always significant wave heights during the test. Initial application of ray-trace models, using the *EOSTAR* propagation assessment tool, predicts that mirage images do not occur for the geometric and environmental conditions during the test (fig. 6).

# 5 Sub-Refractive Mirages are Common in the Marine Environment

The methods and analysis available within the *EOSTAR* model are applicable to a wide range of propagation conditions. In the next two sections we will concentrate on sub-refractive conditions and the exploitation of mirage images. Sub-refractive conditions occur essentially when the air temperature at some small height above the surface is less than the

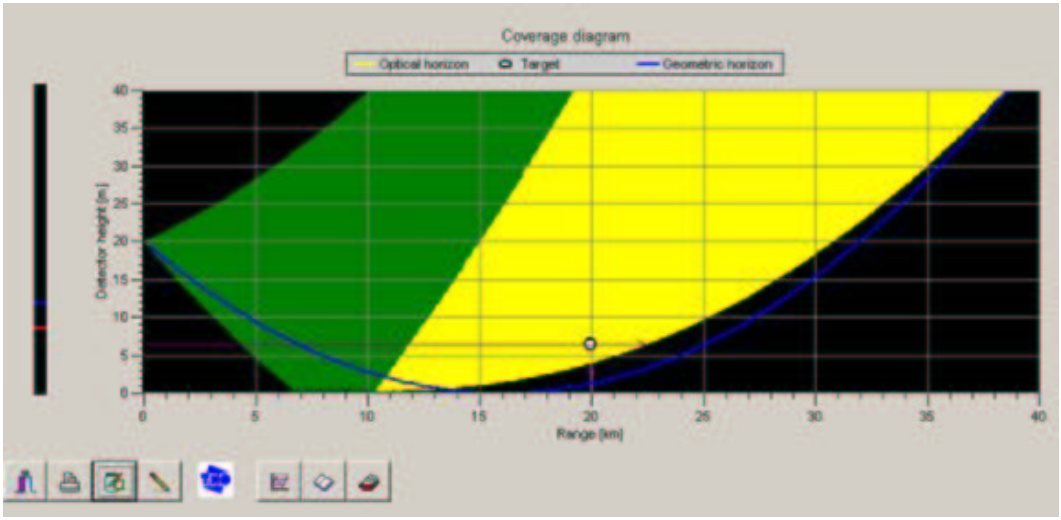


Figure 5: This coverage diagram depicts the field-of-view of the sensor in a two-color coding; targets in the green zone will generate a single image (no mirage), whereas targets in the yellow zone may generate two separated images.

sea temperature: $(T_{\text{air}} - T_{\text{sea}} < 0)$. To get a rough idea of the probability of occurrence of $T_{\text{air}} - T_{\text{sea}} < 0$, a survey of $8,088,855$ shipboard measurements from the Ducting Climatology Survey over 273 Marsden squares worldwide reveals that $T_{\text{air}} - T_{\text{sea}} < 0$ for more than 89% of the samples. The remainder of this section develops a result for passive ranging given the existence of sub-refractive conditions.

The ray-trace algorithm first defines the vertical profile as a set of discrete layers, each with a characteristic temperature and refractivity gradient. A characteristic radius of curvature is then assigned to each layer using eqn. (4) above. The conditions for a sub-refractive mirage require a surface temperature relatively warmer than the air temperature a short distance above the surface. Monin-Obukhov similarity theory can be applied to deduce the vertical temperature profile for this situation, since the Richardson number is negative and unstable conditions apply. The form of the vertical temperature gradient given by similarity theory is

$$\frac{dT}{dz} \propto \ln\left(\frac{z}{z_0}\right) \tag{8}$$

where $z$ is the height above the surface. Thus $dT/dz$ has a large negative value very near the surface and it increases toward zero as height increases. Consider a fixed value of $\lambda$ and a constant air pressure as well, since the pressure variations as a function of height can be neglected for the geometry of interest here, $(0 \leq z \leq 50$ meters), so eqn. (2) can be written

$$\frac{dn}{dz} = \frac{-C_0}{T^2}\left(g\beta + \frac{dT}{dz}\right) \tag{9}$$

This shows that $dn/dz$ is large and positive very near the surface, and that it decreases monotonically as z increases.

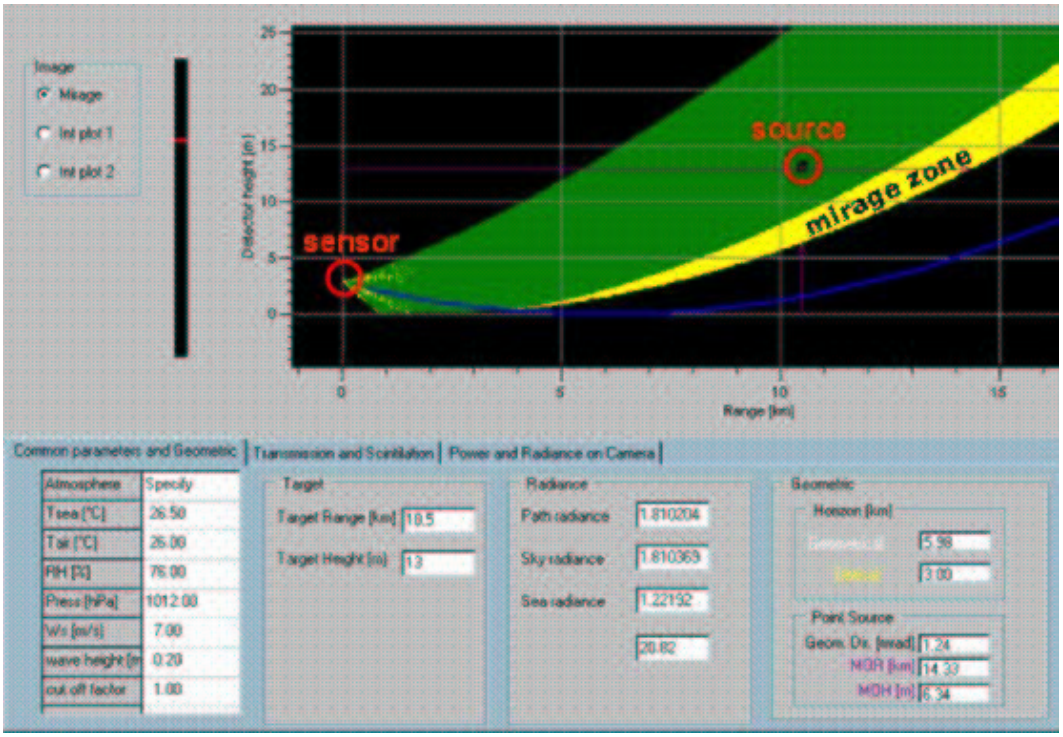


Figure 6: An example of the use of the *EOSTAR* tool to predict the region of mirage occurrence (in yellow), and the region of no mirage (green zone). In this simulation of the test geometry from the Rough Evaporation Duct test, the source is in a no-mirage zone.

The vertical temperature profile defines a set of layers $\sigma_1 \ldots \sigma_u$ with $\sigma_1$ denoting the layer nearest the surface. A temperature and a height are determined for each layer boundary, and associated with each layer $\sigma_i$ is a vertical thickness $\Delta z_i$. Within each layer $\sigma_i$ there is an associated temperature gradient $\nabla T_i = (dT/dz)_{z \in \sigma_i}$. From this we determine a refractivity gradient $\nabla N_i = (dn/dz)_{z \in \sigma_i}$, and finally by the calculation in eqn. (4) an associated radius $r_i$. For sub-refractive conditions, $T_1 > T_2 > \ldots > T_u$. Because of eqn. (8) and eqn. (9)

$$|\nabla N_1| > |\nabla N_2| > \cdots > |\nabla N_k| \tag{10}$$

and

$$|r_1| < |r_2| < \cdots < |r_u| \,. \tag{11}$$

Since $dn_i/dz < 0$ and $r_i < 0$ for all the layers, all rays will be concave upward. The implication for a ray calculation in sub-refractive conditions is that the radius of curvature of a ray decreases as the height above the surface decreases.

## 6 Using Multiple Mirage Images to Find Height and Range

During sub-refractive mirage conditions, an imaging sensor will record two distinct images of a single point source. In previous studies it has been shown [5, 6] that the two images can be exploited to provide both height and range information. We will now show how the ray-trace procedure within *EOSTAR* creates a coordinate transformation.

In fig. 1 a receiver has been positioned at a height of 15 meters, and the set of rays tracing the propagation path defines an envelope. The ray envelope has an intersection structure with a set of constant-height surfaces at heights of $2, 4, 6, 8, 10$, and 12 meters. A ray traced from the receiver intersects a given constant-height surface either once, twice, or not at all. The intersection structure of the constant-height surfaces with the ray-trace envelope induces a transformation.

The result of this transformation is shown in fig. 7. We define an isomet surface as a surface of constant height, and we will use the term *isomet* to refer to the contour curves representing the intersection set between a constant-height surface and the ray-trace envelope shown in fig. 7. Each of the isomets in fig. 7 displays a similar form. The vertical axis shows angular displacement from the horizontal tangent plane at the sensor. The horizontal axis shows range.

The graph of a single isomet can be interpreted by imagining a source confined to one of the isomet surfaces shown in fig. 1 Consider a source on the 12 meter isomet) as it moves toward the sensor from the 25 km range. At $\approx 23.5$ km, the source appears over the horizon as a single point which immediately splits into two images. As seen through an imaging sensor, for example, one image decreases in angular elevation, and the upper image increases in angular elevation as the source moves closer in range. This information is depicted in fig. 7 and corresponds to the outermost curve labelled "12 m". At $\approx 11.5$ km, the lower image descends below 2.8 milliradians: in terms of the imaginary sensor, it has descended beneath the lowest edge of the sensor focal plane. The (now solitary) upper image continues to rise to the upper edge of the sensor field-of-view.

Within the last 6 km, the source is seen to rapidly move from near the top edge to disappear below the bottom edge. The shape of the 12 m isomet is characteristic of all the isomet contours for surfaces of height *less* than the sensor height. When the isomet surface height is greater than sensor height, an inbound upper image disappears across the upper boundary, and never re-crosses from top to bottom.

The key to a deduction of height and range from angular elevation information is the utilization of those portions of an isomet for which two values of elevation correspond to a single range value. Thus for the $12-$meter isomet, ranges between 11.5 km and 23.5 km correspond to two distinct elevation values. This indicates that it is possible to find a one-to-one correspondence between a pair of elevation angles, and a height-range pair.

The actual transformation from the (lower angle, upper angle) coordinate space to the (height, range) coordinate space is shown in fig. 8. When two images are detected by a sensor, the elevations of the lower and upper images can be plotted as a point in fig. 8, and the height and range of that point can be read from the inner coordinate system. To say it

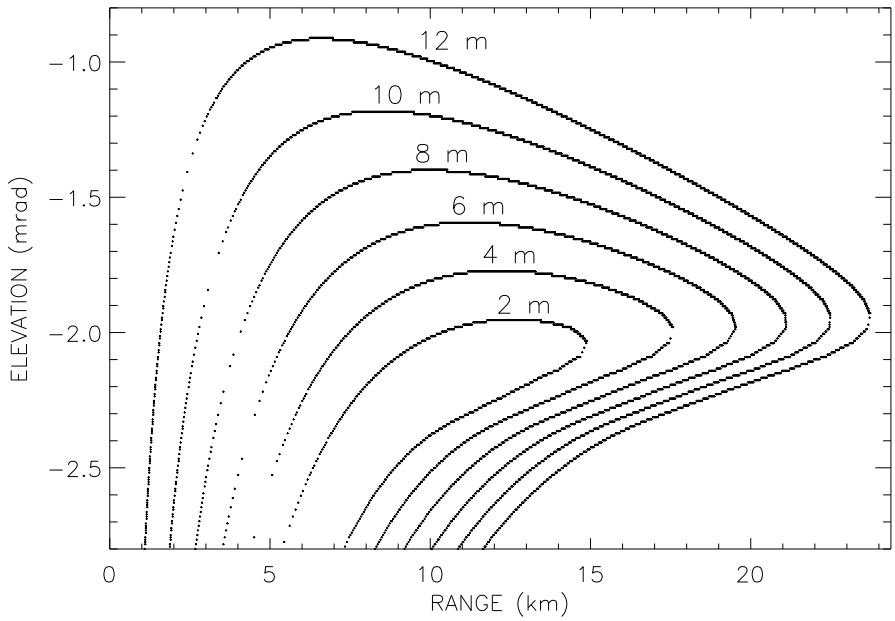


Figure 7: A series of isomets at the heights of $2, 4, 6, 8, 10$, and $12$ meters. For a given range value, each isomet defines either $0, 1$, or $2$ corresponding elevation values.

differently, the figure contains the transformation which takes two elevation measurements as input, and generates as output both height and range of the source or target. In terms of coordinate systems, the rectilinear lower elevation vs upper elevation coordinate system is transformed to the distorted, curvilinear height vs range coordinate system.

Consider as an example an imaging sensor system with a telescope which detects a source in a sub-refractive mirage regime. The two elevations can be determined from the imaging frame: suppose $(\phi_{\text{lower}}, \phi_{\text{upper}}) = (-2.65, -1.6)$. The transformation displayed in fig. 8 shows the actual range and height can be read out from the transformed coordinate system yielding range $\approx 10$ km, and height $\approx 6$ m.

## 6.1 Potential for Application

As we noted above, sub-refractive conditions are quite common for the marine atmospheric surface layer. For our imaging geometry, these conditions cause mirages that appear at two different elevations. The usable range for the particular example presented here is from 9 km out to $\approx 18$ km. Note that the range limits for effective range-finding are determined by the intensity of the sub-refractive conditions and by sea-surface roughness. As air-sea temperature difference $T_{\text{air}} - T_{\text{sea}}$ becomes more negative, the range domain for which two images occur increases in extent by moving the point of first appearance of two images closer to the sensor. Conversely, as air-sea temperature difference $T_{\text{air}} - T_{\text{sea}}$ becomes less negative

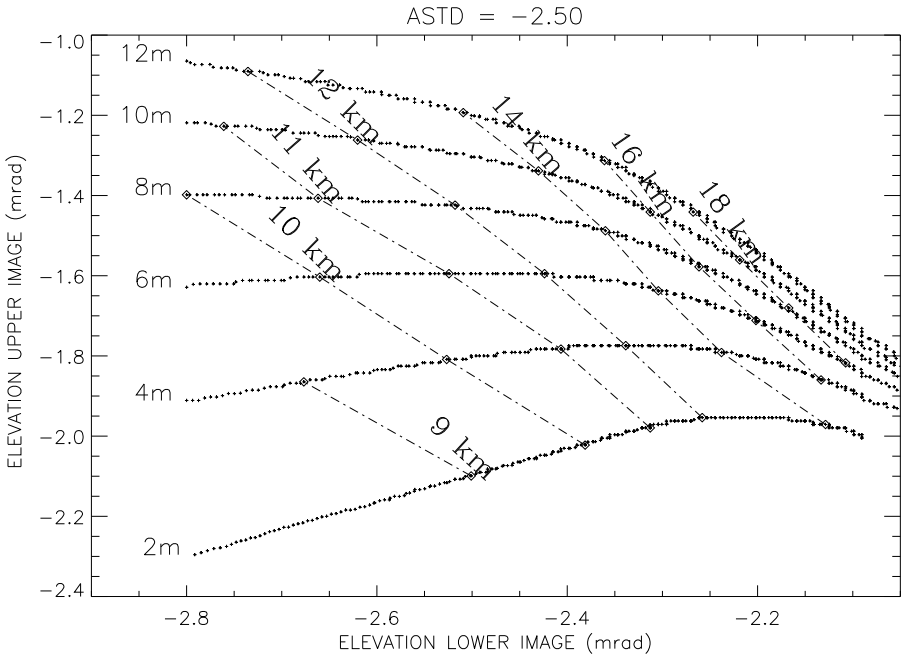


Figure 8: The transformation that is implied by the data in fig. 7. The same information is shown here, but restricted to the portions of the isomets that are dual-valued. For example, the angular elevation pair $(\phi_{\text{lower}}, \phi_{\text{upper}}) = (-2.65, -1.6)$ transforms to a range $\approx 10$ km and a height $\approx 6$m.

and closer to zero, the range domain for which two images occur decreases in extent: the first appearance of two images occurs at a point further away from the sensor. A rough sea surface will occlude the lowest height rays which will also force the point of first appearance of mirages further away from the sensor.

# 7 Conclusions

The *EOSTAR* propagation prediction model is an integrated model suite for a diverse set of maritime infrared and optical propagation scenarios. It provides many of the essential tools for an end-to-end performance prediction.

The primary strength of the *EOSTAR* tool is the possibility to run through a sequence of parameter values to visualize the effects on the model output. This permits a fully interactive approach to any testing of parameter variation on the final transmission values. The model uses a geometric optics approach to the problem of characterizing sources or targets at long range within the marine atmospheric surface layer.

The ray method also provides a useful framework for the calculation of other path-dependent signal metrics such as molecular and aerosol extinction, scintillation and the refractive index structure function $C_n^2$.

## References


[1] Lehn, W., *Appl. Math. Model.* **9,** 447, 1985.

[2] Doss-Hammel, S. M., Zeisse, C. R., Barrios, A. E., de Leeuw, G., Moerman, M., de Jong, A. N., Frederickson, P. A., Davidson, K. L., "Low-Altitude Infrared Propagation in a Coastal Zone: Refraction and Scattering", Applied Optics, **41**, 3706–3724, 2002.

[3] Kravtsov, Y., and Orlov, Y., *Geometrical Optics of Inhomogeneous Media*, Springer-Verlag Berlin, 1990.

[4] Kravtsov, Y., and Orlov, Y., *Caustics, Catastrophes and Wave Fields*, Springer-Verlag Berlin, 1999.

[5] Trahan, J., and Rivera, H. "Mid-wave infrared low elevation propagation experiment on the Potomac River, Summer 1995", Technical Report NSWCDD/TR-96/23 (Sept. 1996).

[6] N. Platt, S. Hammel, J. Trahan, H. Rivera, "Mirages in the marine boundary layer – comparison of experiment with model", *Proc. IRIS Passive Sensors*, Monterey, CA, vol. 2, 195-210, 1996.